Desenvolvimento de um secador solar de leito fixo: estudo experimental e simulação CFD

Development of a fixed bed solar dryer: experimental study and CFD simulation

Desarrollo de un secador solar de lecho fijo: estudio experimental y simulación CFD

Ana Carolina Ribeiro Stoppe

ORCID: https://orcid.org/0000-0002-4744-0738

Universidade Federal do Triângulo Mineiro, Brasil

E-mail: anacarolina_stoppe@hotmail.com

José Luiz Vieira Neto

ORCID: https://orcid.org/0000-0003-0736-3974

Universidade Federal do Triângulo Mineiro, Brasil

E-mail: jose.neto@uftm.edu.br

Kássia Graciele dos Santos

ORCID: https://orcid.org/0000-0001-7452-6900

Universidade Federal do Triângulo Mineiro, Brasil

E-mail: kassia.santos@uftm.edu.br

Resumo

Diante do desafio de desenvolver secadores solares mais eficientes, a técnica de Fluidodinâmica Computacional (CFD) foi aplicada neste trabalho para testar diferentes configurações de entrada de ar em um secador solar de leito fixo, com entradas laterais. Por meio das simulações, foi determinada a melhor configuração de alimentação de ar que favoreceu o contato entre partículas. Foi construído um secador solar de leito fixo, no qual se realizou experimentos com sementes de soja e folhas de *Moringa oleífera LAM*. Duas configurações de alimentação de ar no secador foram testadas: entradas totalmente abertas e parcialmente abertas. Os resultados de CFD mostraram que a vazão de ar foi mais pronunciada no topo do leito, perto do exaustor, quando a alimentação de ar ocorre por entradas laterais totalmente abertas ao longo do leito. Isso pode explicar os resultados experimentais de secagem, em que os materiais apresentaram uma secagem heterogênea, secando de forma mais eficiente no topo do leito. De acordo com as simulações, o perfil de velocidade de ar passa a ser mais homogêneo quando o ar é alimentado apenas na base do

leito. Assim, a secagem na configuração parcialmente aberta foi mais homogênea, e com taxa de secagem cerca de 300% superior à obtida na condição com entradas totalmente abertas.

Palavras-chave: Secagem solar; Sustentabilidade; *Moringa oleífera*; Folhas; Soja.

Abstract

Facing the challenges to develop more efficient solar dryers, this work used the Computational fluid dynamics (CFD) to test different configurations of lateral air feeding in a fixed bed solar dryer. Through the simulations, it was found the best configuration of air inlet that provided a better fluid-particle contact. It was made a fixed bed solar dryer, which was tested using soybeans seeds and *Moringa oleifera LAM* leaves to evaluate the drying rate using two bed configurations: fully opened and partially opened inlets. The CFD results indicated that the air flow rate was more pronounced at the bed top, near the exhaust fan. This can explain the poor drying near the bottom for the experiments performed with all lateral inlets opened. According to the simulation results, the air velocity profile was more homogeneous when the air was fed only near the bottom. So, the use of a partially opened configuration led to a more homogenous solar drying, with a drying rate about 300% higher than the one using the fully opened inlets.

Keywords: Solar drying; Sustainability; *Moringa oleifera*; Leaves; Soybeans.

Resumen

Ante el desafío de desarrollar secadores solares más eficientes, la técnica de dinámica de fluidos computacional (CFD) se aplicó en este trabajo para probar diferentes configuraciones de entrada de aire en un secador solar de lecho fijo con entradas laterales. A través de las simulaciones, se determinó la mejor configuración que favoreció el contacto entre partículas. Se construyó un secador solar de lecho fijo, en el que se realizaron experimentos con semillas de soja y hojas de *Moringa oleífera*. Se probaron dos configuraciones en la secadora: entradas de aire completamente abiertas y parcialmente abiertas. Los resultados de CFD mostraron que para entradas de aire completamente abiertas, el flujo de aire era más pronunciado en la parte superior de lo lecho, cerca del fan. Esto puede explicar los resultados experimentales de secado, en los que los materiales presentaron un secado heterogéneo, más eficiente en la parte superior del lecho. Según las simulaciones, el perfil de velocidad del aire se vuelve más homogéneo cuando el aire se alimenta solo en la base del lecho. Por lo tanto, el secado en la configuración parcialmente abierta fue más homogéneo, y con una tasa de secado alrededor de 300% más alta que la obtenida en la condición con entradas completamente abiertas.

Palabras clave: Secado solar; Sostenibilidad; *Moringa oleífera*; Hojas; Soja.

1. Introduction

In 2017, the annual average solar radiation at the southeast of Brazil was about 4.95 kWh·m^{-2} (INPE, 2017), which demonstrates the high potential of solar energy application as solar drying, both in domestic and industrial sectors. In addition, this region has an intensive grain harvest and generates a large amount of crop residues, which eventually need to be dried. An example is the soybean seeds (SS) production, which requires the seeds to be adequately dried to ensure appropriate water content for commerce and increase their post-harvest conservation potential, maintaining their physical proprieties (Souza et al., 2015a, Souza et al., 2015b).

Another important dried product commercialized as nutrient supplement is the *Moringa oleifera* Lam. (MOL), also called drumstick tree or horseradish tree. This plant is indigenous to northwestern India (Perumal & Klaus, 2003; Olabode et al., 2015) and is common in Southeast Brazil. The MOL is classified as a multifunctional plant, as it has become increasingly widespread in animal and human food; it is also used in the cosmetic and pharmaceutical industries; for the production of oil, soap, fertilizers and biopesticides; as an additive for clarifiers; surfactants (Andrade et al., 2020) and for sewage and water treatments (Santos et al., 2019; Perumal & Klaus, 2003).

The most consumed and nutritious part of MOL is its leaf, which is a rich source of vitamins A, B, and C (Câmara et al., 2019); essential amino acids such as methionine, cystine, tryptophan, and lysine; beta-carotene; proteins; and minerals such as Fe, K, Ca, and Zn (Olabode et al., 2015). Moreover, dried MOL contains about 10 times more vitamin A than carries, 17 times more Ca than milk, 18 times more K than bananas, and 25 times more Fe than spinach. This elevated level of nutrients makes the MOL an excellent option as a nutrient supplement (Perumal & Klaus, 2003). However, the Moringa leaf is highly perishable due to the elevated moisture content (about 74% w/w). Therefore, the leaves are usually dried to extend their shelf life (Olabode et al., 2015).

During the drying operations, two processes take place. First, heat is transferred from the surrounding medium to the particle, resulting in liquid evaporation on the material (Rigueto et al., 2020). Then, mass transfer of liquid (or vapor) occurs from inside the particle to the particle surface and finally from this surface to the drying fluid stream. So, the kinetic of drying can change according to the materials structure and needs to be studied for each

material individually (Barros et al., 2020; Gomes et al., 2020; Santos et al., 2020a; Santos et al., 2020b; Almeida et al., 2020).

Several papers report the use of solar drying systems related to food products (Ratti & Mujumdar, 1997; Leon & Kumar, 2008; Akbulut & Durmuş, 2010; Agrawal & Sarviya, 2016; Atalay et al., 2017) . The traditional open sun drying technique has been the most usual and cheapest approach. However, some major disadvantages associated with the open sun processes have been reported (Agrawal & Sarviya, 2016), such as a longer drying time, contamination, difficulty in controlling the process, loss of natural color and mineral, infestation by insects and birds, adverse weather conditions, large drying area requirement, and elevated labor costs. All these limitations of open sun drying have led to the development of other solar dryer devices.

The fixed-bed dryer has been widely used in drying processes of agricultural products, motivated by the low initial investment and operating cost, as well as its easy operation. Considering the economic and social points of view, fixed beds are one of the cheapest equipment to build and consist an excellent alternative for small and medium-sized rural properties; moreover, they can be easily installed on a property or in a rural cooperative (Silva et al., 2019).

The packed beds (or fixed beds) promote direct particle-fluid contact and allow to control the drying process variables, such as airflow rate, temperature, and material weight. Since the packed bed is a dense granular system, the heat- and mass-transfer resistances are pronounced; thus, a detailed study of the fluid dynamics of the airflow in a porous media is required to guarantee the quality and standardization of the final product (Souza et al., 2015b).

Silva et al. (2013) studied the drying of pineapple residues in a thin-layer fixed-bed dryer and the effect of the process variables on the antioxidant properties. They observed that the content of some bioactive compounds increased after the drying. Souza et al. (2015b) dried SSs in a fixed-bed dryer heated by electrical resistance and evaluated the effect of the process heterogeneity on seed quality. This heterogeneity occurs because the particles near the inlet receive the hotter and drier air, drying faster than those near the outlet.

Silva et al. (2019) numerically and experimentally investigated the heat and mass transfers during the acerola residues drying in a deep fixed bed and found a heterogeneity on the product. This shows that only one air feed at the bottom is not the best configuration to produce a homogeneous dried product. Therefore, new investigations are needed to improve the particle-fluid contact and also to reduce the energy cost during the drying process.

Regarding the solar drying using fixed beds, Mardiyani et al. (2019) developed a convective ecofriendly fixed-bed solar dryer working with one air inlet and using five trays with 7 cm of packed material. The drying of red pepper required about 5–6 days to dry the first tray, 8–9 days for the second tray, and 9–10 days for the third tray, until 12% (*w.b.*) of moisture was achieved. Therefore, the drying process took some days, which shows the necessity to better investigate the phenomena that take place in the fixed-bed dryer using solar energy.

With the advances in computational resources, the numerical simulations using Computational fluid dynamics (CFD) can help shed light on the airflow patterns in fixed beds, allowing to propose some modifications in order to improve the equipment efficiency (Santos et al., 2012).CFD simulations have been outstanding in the analyses of heat, mass, and momentum transfers phenomena in diverse equipment, such as spouted beds (Cunha et al., 2009; Vieira Neto et al., 2008; Santos et al., 2015; Santos et al., 2017; Bortolotti et al., 2013); fluidized beds (Araújo & Santos, 2017; Müller et al., 2009); fixed beds (Béttega et al., 2013); hydrocyclones (Vieira et al., 2016); rotational disk granulators (Vieira Neto et al., 2017); dryer drums (Cunha et al., 2016; Silvério et al., 2014); and solar dryers (Krawczyk & Badyda, 2011; Tegenaw et al., 2019).

According to Tegenaw et al. (2019), the CFD technique is a promising design and modeling tool that can provide important information in cases where experimentation is limited, reducing costly experimental trials. The computational simulations are successfully used to predict air velocity profiles, temperature, and moisture within the dryer, allowing to examine and interpret the different operating conditions without an extensive set of experimental tests.

The CFD technique has been contributing to the design of new equipment and the optimization of existing dryers, which ensures a better final product, under suitable processing and storage conditions. Krawczyk & Badyda (2011) proposed a model based on the heat and mass-transfer phenomena in a drying process. The authors considered the application of boundary conditions on the material surface and the physical boundary between the air and the solid phase (dry material) and calculated the dryness and humidity as a function of dryer position.

Tegenaw et al. (2019) used a CFD model to predict the airflow patterns and transient heat transfer within a truncated pyramid-shaped solar dryer. The simulations revealed higher values of air velocity (about 0.5 m·s⁻¹) near the exhaust fan. The spatial

temperature distribution was uniform after 30 min of solar exposure, reaching a maximum temperature of 60°C.

Béttega et al. (2011) performed mathematical simulations of radial heat transfer in packed beds using pseudo-homogeneous modeling. Béttega et al. (2013) studied the heat transfer inside a packed bed of glass beads with heat source located on the wall of the equipment from a 2D model. Different profiles were evaluated for the voidage distribution along the radial direction of the bed and its effect on the behavior in the whole device. From this approach, the authors determined the temperature distribution at the outlet for different fluid velocities, using physical parameters of the phases present in the system. Comparing the CFD results with experimental data and other models from the literature, the capacity of the model and the numerical procedure adopted to represent the phenomenon were verified.

In the present study, a sustainable solar dryer was designed for drying different agricultural materials, such as SS and MOL leaves, with low cost and high efficiency. For this, new different configurations of a fixed bed were evaluated by CFD simulations. It was studied the effect of different settings of airflow inlets over the air velocity profile along the fixed bed, to find a condition that improves the particle-fluid contact and also the heat and mass transfers. Then, two configurations were tested experimentally to capture the influence of the climatic conditions over the drying processes. The mathematical model and initial condition used for the CFD simulations are detailed in the next section, as well as the experimental procedure used in the drying experiments. The experimental results were analyzed, and the discussion was supported by the simulation results and literature works.

2. Mathematical modeling

A porous media model can be used for a wide variety of problems, single-phase or multiphase systems, including flow through packed beds, filters, and perforated plates. In this study, when this model was used, a cell zone was defined where it was applied, and the pressure drop in the flow was determined through its inputs, being described by the momentum equation in the porous media. Heat transfer through the medium might also be represented, with or without the assumption of thermal equilibrium between the solid and the fluid, modeled by the energy equation in a porous media.

The porous media model incorporated a flow resistance determined empirically in a region of the system defined as porous. In essence, this model added a dissipation term to the momentum equation. Consequently, some hypotheses were assumed in the model, and its

limitations might be recognized (Béttega et al., 2011), such as a 2D transient axis-symmetric model, where the porous media momentum resistance and heat source terms are calculated separately on each phase; the assumption of isotropic porosity and an initial air velocity at the entrance of 0.98 m·s⁻¹ at 338.15 K. Since the block generated by the porous medium that was physically present was not represented in the model, the ANSYS Fluent 17.2 Standard reported a surface velocity inside the porous medium, to ensure the continuity of the velocity vectors through the interface of the porous medium. A more representative alternative in which the mean interstitial velocity was calculated inside the porous medium was chosen, and in this way, the voidage was included in the differential terms of the transport equations.

The set of conservative and constitutive equations for the fluid in a porous media, as presented in Table 1, were solved by the finite-volume method. Assuming isotropic voidage and a single-phase system, the continuity and momentum equations could be described by Eqs. (1) and (2), respectively.

Table 1 – Conservative Equations solved to simulate the air flow in the porous media.

(A) Continuity for fluid phase in the porous media	Equations:
$\frac{\partial}{\partial t}(\varepsilon\rho) + \nabla\cdot(\varepsilon\rho\vec{v}) = 0$	(01)
(B) Momentum Conservation for the fluid phase flowing in the porous media	
$\frac{\partial}{\partial t}(\varepsilon\rho\vec{v}) + \nabla\cdot(\varepsilon\rho\vec{v}\vec{v}) = -\varepsilon\nabla p + \nabla\cdot(\varepsilon\vec{\tau}) + \varepsilon\vec{B}f - \left(\frac{\varepsilon^2\mu}{K}\vec{v} + \frac{\varepsilon^3 C_2}{2}\rho|\vec{v}|\vec{v}\right)$	(02)
(C) Source term for the homogeneous porous media, Si:	
$S_i = -\left(\frac{\mu}{\alpha}v_j + C_2\frac{1}{2}\rho|v|v_j\right)$	(03)
(D) Ergun Equation for the for the pressure drop in a porous media (turbulent regime):	
$\frac{|\Delta p|}{L} = \frac{150\mu}{D_p^2}\frac{(1-\varepsilon)^2}{\varepsilon^3}v + \frac{1,75\rho}{D_p}\frac{(1-\varepsilon)}{\varepsilon^3}v^2$	(04)
(E) Constitutive equation for permeability in the porous media (ERGUN, 1952):	
$\alpha = \frac{D_p^2}{150\mu}\frac{\varepsilon^3}{(1-\varepsilon)^2}$	(05)
(F) Constitutive equation for the inertial loss coefficient in the porous media:	
$C_2 = \frac{3,5}{D_p}\frac{(1-\varepsilon)}{\varepsilon^3}$	(06)
(G) Constitutive equation for the viscous resistance of porous media:	
$Rv = \frac{150\,(1-\varepsilon)^2}{\Phi^2 Dp^2\varepsilon^3}$	(07)
(H) Constitutive equation for the inertial resistance of porous media:	
$Iv = \frac{3,5\,(1-\varepsilon)}{\Phi\,Dp\,\varepsilon^3}$	(08)

The inputs of the resistance coefficients were assumed to be based on well-established empirical correlations, which have been usually based on surface velocity. Thereby, the inputs of resistance coefficients were automatically converted to those that were compatible with this formulation. Consequently, the homogeneous porous medium was modeled by adding a source term S_i, as shown in Eq. (3), in the continuity and momentum equations (Béttega et al., 2013).

In a turbulent flow, the fixed bed was modeled using both the permeability and inertial loss coefficient. For this, Ergun's equation could be used, as shown in Eq. (4) (Ergun, 1952). The permeability (α) and the inertial loss coefficient (C_2) in each component may be identified by Eqs. (5) and (6), where ε is the voidage; D_p is the particle diameter (m); and ϕ is the particle sphericity, obtained experimentally.

The mathematical model for heat transfer simulation adopted by ANSYS Fluent 17.2 used the energy equation, i.e., Eq. (7), with some modifications in the conductive transport of heat and in the transient terms, specifically for the case of the porous media. The morphological proprieties of SSs and MOL leaves, such as the mean diameter of Sauter, apparent density, and sphericity, need to measured experimentally to calculate the packed bed properties: voidage, permeability, and the inertial resistance factor.

3. Material and Methods

Experimental Apparatus

The fixed-bed solar dryer developed in this work is presented in the Figure 1. The equipment consists of a black fixed bed (A) (absorber body) located inside a solar furnace cabin, which consists of a metal support (B) covered by a glass box (C) to create a greenhouse effect. A radiator (D) was painted black and inserted between the metal support and the fixed bed to increase the metallic surface area that absorbs the solar radiation and transfers heat to the air. Two side plates covered by a reflective film (F) were added to increase solar radiation uptake. Behind the metallic support, a thermal insulation (G) was design to avoid thermal losses. The fixed-bed geometry was a rectangular vessel with an exhaust fan at the exit (E) to promote the air suction through the several lateral inlets (Figure 1b), with 0.01 m across the bed. These lateral entrances could be closed, allowing many airflow inlet configurations: fully open configuration (FO); alternating airflow inlets (AAI); unilateral airflow inlets (UAI) and a partially open bed (PO), with only the first 3 inlets open.

Figure 1 – Experimental device: (a) detailed schematic diagram with: A- fixed bed; B- metallic support; C- glass cover; D- extended surface; E- exhaust fan; F- reflector; G-thermal insulation; (b) fixed bed with 8 lateral air inlets.
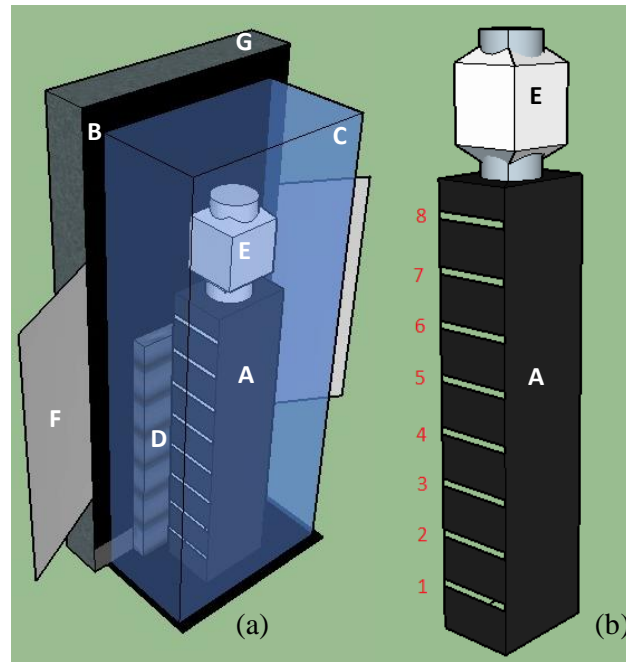
Particle Characterization

To calculate the porous media properties, all particles were submitted for characterization, with all analyses in triplicates. The mean volumetric diameter for SSs was calculated by 3D measurements taken with a pachymeter. Therefore, their volume was determined by assuming an ellipsoidal form, using a sample of 30 particles. These particles were then weighed, and the apparent density was calculated by the weight-to-volume ratio of the sample.

Regarding the MOL particles, fresh samples were collected daily since the leaves rapidly lose their freshness. The weight, thickness, and a projected area of 20 samples (with 15 leaves each) were measured and recorded to estimate the apparent density. Therefore, the volume was the product between the projected area and thickness. The voidage was calculated considering the particles weight packed in the fixed bed.

Simulation Conditions

Some CFD simulations were performed to analyze the influence of different inlets arrangements over the air velocity profile through the packed bed. The airflow inlets at different assemblies are showed in Figure 2: all airflow inlets open, named as the fully opened

(FO) configuration (Figure 2a); the alternate airflow inlets (AAI), shown in Figure 2b; unilateral airflow inlets (UAI), as presented in Figure 2c; and the configuration of five airflow inlets closed at the top, while only three inlets are opened at the bottom; this configuration is named the partially opened (PO) configuration, as shown in Figure 2d.

Figure 2 – Different settings of airflow inlets: (a) fully open configuration (FO); (b) alternating airflow inlets (AAI); (c) unilateral airflow inlets (UAI); (d) partially open bed (PO), with only the first 3 inlets open.

(a)   (b)   (c)   (d)
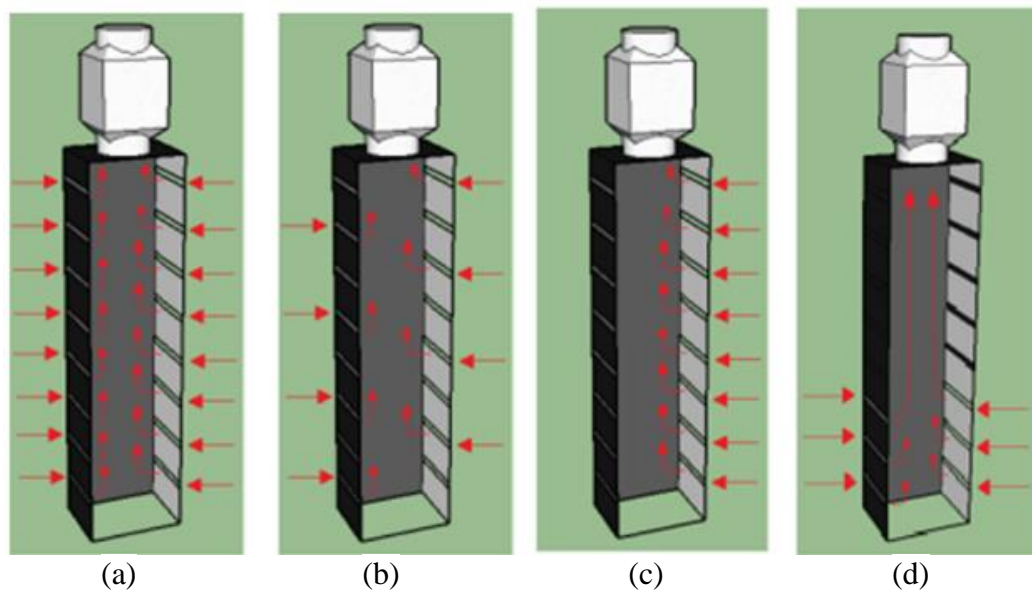
A 3D computational grid was generated for the dryer, a rectangular based vessel (0.10 m × 0.15 m) with 0.60 m height, using the Gambit® software. Before the simulations, a mesh independence test was performed. The final mesh was about 220,502 elements, with hexahedral cells along the bed and tetrahedral cells near the exhaust fan.

The simulations were performed using ANSYS Student Fluent 17.2 software. The momentum and continuity equations for the fluid phase were solved using the finite-volume method, considering that this fluid permeated a porous medium, and the media properties were obtained experimentally.

The conditions adopted in CFD studies are described in Table 2. The fluid consisted of air at 60 ℃ (maximum temperature found experimentally), while the particles were considered as a porous zone. The values for the viscous and inertial resistances of the porous media were calculated by Eqs. (6) and (7), which were derived from Ergun's equation, in Table 1 (Ergun, 1952).

Table 2 also shows the conditions simulated in this work, all them for packed beds with an initial static bed height of 0.57 m. Simulations 1 to 4 were realized for the SS in order to evaluate the influence of different air inlet settings on the fluid paths inside the fixed bed, for outlets air velocities of 0.5, 1, and 2 m·s^{-1}. Thus, a fixed bed filled with SS (Case 1) were simulated for all arrangements in Figure 2. Afterward, some simulations were performed for the FO bed and PO bed, using *Moringa oleifera* leaves (Case 2). Simulations 5 and 6 were done for a packed bed of MOL leaves, operating with the FO and PO air inlet configurations, at an outlet air velocity of 2 m·s^{-1}.

Table 2 – Particles proprieties and operational conditions used in CFD simulations.

Sim.	Inlet Configuration	Proprieties of particles						Resistances [$1·m^{-2}$]	
		Particles	ρ_p [kg·m^{-3}]	ε	(ϕ)	Dp [m]	Shrinkage [%]	Viscous R_υ	Inertial I_υ
S1	FO (at 0.5, 1, 2 m·s^{-1})								
S2	AI (at 0.5, 1, 2 m·s^{-1})	SS	1289	0.370	0.900	0.006	-	3.861·10^7	7.80·10^3
S3	UI (at 0.5, 1, 2 m·s^{-1})								
S4	PO (at 0.5, 1, 2 m·s^{-1})								
S5	FO (at 2 m·s^{-1})	MOL	546	0.679	0.435	0.015	19.5	1.244·10^6	5.70·10^2
S6	PO (at 2 m·s^{-1})								

Experimental procedure of solar drying tests

Before the drying tests, the air velocities of the empty and packed bed were measured along the axial position to check the effect of the obstruction of the five top air inlets over the airflow inside the bed.

The experiments were carried out on sunny days, from May to June 2017, which covered the autumn and winter seasons in Uberaba, Brazil. The developed solar dryer was positioned facing the north, in an open area near an automatic weather station of the Brazilian National Institute of Meteorology at Uberaba, MG, Brazil (47°93' W; 19°77' S). The meteorological data, including solar radiation and wind velocities were recorded on site every one hour.

The solar dryer experiments consisted of packing the particles inside the bed until a static bed height of 0.57 m was achieved, which led to an amount of 6.2 kg of SSs and 1.41 kg of MOL (Figure 3a). After that, the equipment was exposed to solar radiation, and the exhaust fan was turned on (Figure 3b).

Figure 3 – Experimental device: (a) fixed bed packed with MOL. (b) experimental apparatus at the beginning of tests.

(a)   (b)

Then, the heated air entered through the side entrances and percolated the porous bed, promoting the transfer of heat and mass that allow drying. The temperatures at the bottom and bed top were recorded every 30 min, as well as the temperatures of the air inside the solar oven and on the glass cover.

Some samples were collected to evaluate the moisture contents at different axial positions of the bed at every 1 h. The samples were weighed and dried at an electric oven for 24 h at 105 °C. From these data, the dry-basis moisture (X_{db}) was calculated using Eq. (9), whereby w_w is the water weight and w_p is the weight of the dried particle. Therefore, Eq. (10) establishes the moisture ratio (*MR*) removed at instant *(i)*; it is also used to describe the kinetics of drying at the packed bed.

$$X_{db} = \frac{w_w}{w_p} \tag{9}$$

$$MR = \frac{X_{db}^i - X_E}{X_{db}^0 - X_E} \tag{10}$$

where X_{db}^i is the moisture in dry basis at time (i), X_E is the equilibrium moisture, and X_{db}^0 is the initial moisture.

Two drying tests using SSs (Case 1) were performed for drying times of 3 and 4 h, only for an FO configuration (Figure 2a). As the drying temperature depends on the weather, Souza et al. (2015b) reported an equilibrium moisture of 0.0678 (d.b.) for SS drying at 40 ºC and an air relative humidity of 35%. These conditions were similar to those found in this work. The initial moisture of SS (X_{bs0}) was about 1.08 (dried base).

The experimental packed bed drying using solar energy with MOL (Case 2) was performed using the FO and PO inlet configurations, and the MRs along the experiments were calculated for a final drying time of 6 h. A dynamic equilibrium moisture was used, obtained by experimental drying tests in an infrared humidity analyzer, at 40 and 60 ℃.

4. Results and Discussions

Particles Characterization

Table 2 also shows the characterization of particulate materials used in this work. The mean diameters were 0.006 m and 0.015 m, with apparent densities of 1289 ± 100 kg·m^{-3} and 546 ± 113 kg·m^{-3} for SS and MOL, respectively. The soybeans were close to a spherical form ($\phi = 0.9$), while the MOL had small sphericity, about 0.435. These lead to a very compacted bed for soybeans, with voidage $\varepsilon = 0.370$ and an extra porous bed for MOL ($\varepsilon = 0.679$), since small particles sphericity leads to a packing with a higher void fraction.

The viscous and inertial resistances of SSs and MOL-packed beds were calculated using the particulate proprieties. It can be seen in Table 2 that small viscous and inertial resistances were found for the MO leaves due to their lower sphericity and higher voidage.

Simulated air velocity profiles

Case 1: The effect of different air inlet settings: To clarify the influence of different air inlet settings on the fluid dynamics inside the fixed bed, some CFD simulations were performed using SS, chosen due their higher sphericity, which brings them closer to a perfect sphere. In addition, soybeans do not suffer much shrinkage when subjected to the drying process.

Figure 4 presents the air velocity contours flowing through the porous bed for all air inlets studied in this work. With increments of outlet air velocity from 0.5 m·s^{-1} to 1.0 m·s^{-1} and 2.0 m·s^{-1}, there was a proportional response in the bed: the velocities of the air that runs through the bed increases, for all bed configurations. Moreover, the air inlets near the exhaust fan showed a higher air velocity than near the bottom, as the packed-bed offers a head loss that increases with the length of the porous medium from the airflow source.

Regarding the different airflow inlets arrangements, the AAI and PO configurations provided more homogeneity of air distribution inside the packed bed, while for the FO configuration, the air was collected only at the top of the bed, due to its proximity to the

exhaust fan outlet. Considering the UAI configuration, the axial air distribution through the bed was heterogeneous, which is not desirable since near the closed inlets, there was no effective contact between air and particles, which could lead to partial drying. The simulations for the PO configuration showed greater air velocities along all axial directions and a better homogeneity; this resulted in higher drying rates during drying.

Figure 4 – Contours of air velocities (m.s^{-1}) for the packed bed with soybeans seeds (SS), obtained by CFD simulations of different inlet configurations: (a) FO; (b) AAI; (c) UAI; (d) PO.
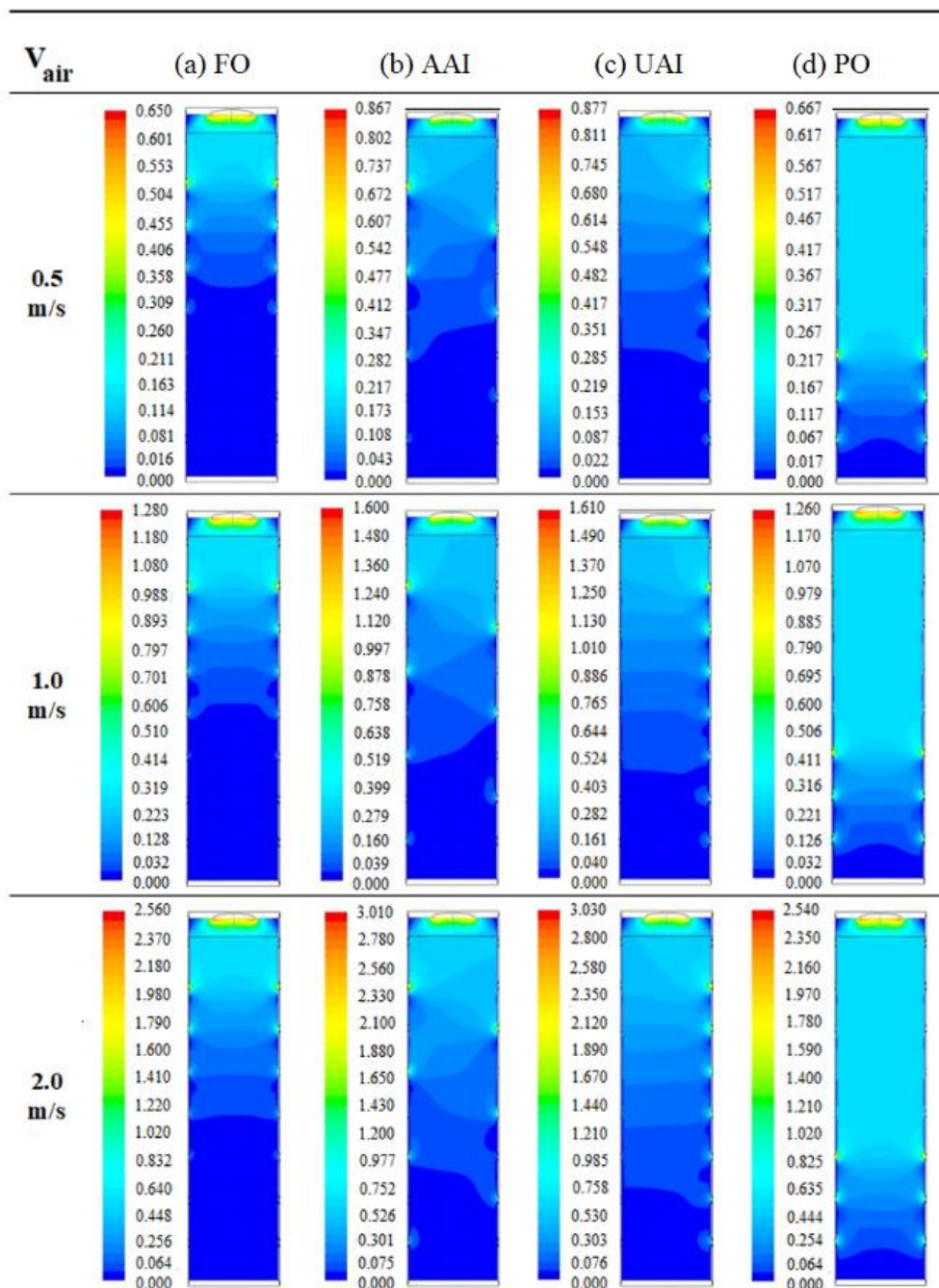
Case 2 – Packed beds operating with MOL particles: CFD simulations were performed to obtain air velocity contours for an MOL-packed bed (FO and PO configurations), which presents a high voidage due to the low sphericity of particles. It can be observed from Figure 5 that a better distribution of airflow took place in the PO configuration because the preferred paths were prevented since the upper entrances were closed. Therefore, the ascendant air had increased velocities even at lower bed heights, providing a more homogenous air distribution and higher particle-fluid velocities. This can improve the heat and mass-transfer coefficients and promote a more efficient drying.

Figure 5 – Contours of air velocities (m/s) for the packed bed with MOL, obtained by CFD simulations of: (a) FO configuration; (b) PO bed.

(a) FO – all airflow inlets open   (b) PO – only three inlets open at bottom
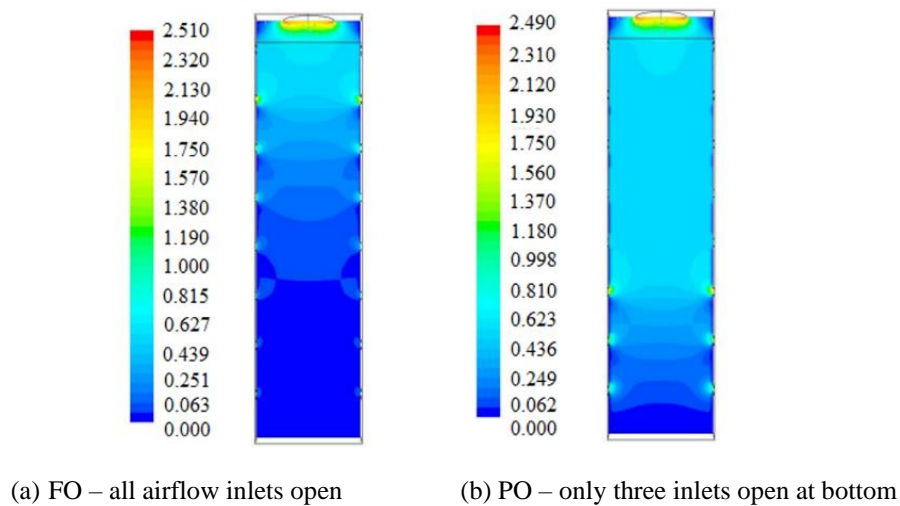
Experimental air velocity profiles

Figure 6 shows the experimental measurements results of axial air velocities along the bed height for the empty bed (a) and an MOL-packed bed (b). The air velocity was verified to increase as it approached the top (Figure 6a), where the exhaust fan was located. However, at the PO configuration, there was a considerable increase in air velocity near the bottom, due to the obstructions imposed in the upper inlets (closed). Hence, the air was forced to get in near the bottom and flow through along the equipment until the exit.

Figure 6b presents the air velocities inside the MOL-packed bed. This behavior was similar to the empty bed, since the PO configuration led to higher air velocities along the bed, but in a more attenuated way when compared with the empty bed, since the presence of particles promoted a higher pressure drop. The dashed lines in Figures 6a and 6b indicate the

last opened air inlet for the PO configuration, where a peak of velocity was verified, probably because this inlet was the closest to the exhaust fan. These experimental results were qualitatively in agreement with the CFD results.

Figure 6 – Experimental airflow velocities measured at different bed heights, for FO (▲) and PO (■) beds: (a) empty bed; (b) bed packed with MOL leaves.
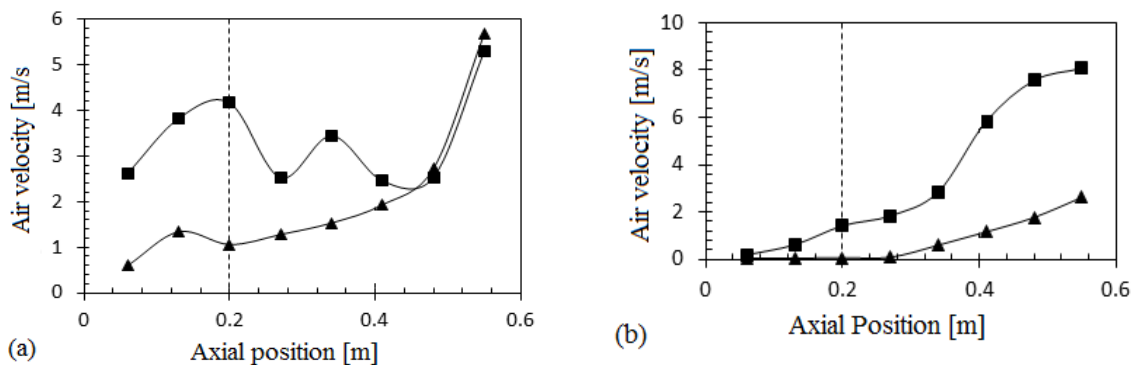
Solar drying tests

Case 1 – Drying of soybean seeds: Experimental drying tests of SSs in PO packed-bed configuration were conducted on sunny days. The environment relative humidity was between 31% and 44% for the experiment with 3 h, while a range of 46%–55% was observed for the test with 4 h.

Figure 7 displays the axial temperatures profiles obtained along the drying experiments of soybeans for experiments with a drying time of 3 h (a) and 4 h (b). The higher temperatures (a maximum of 59 ℃) were recorded for the bed wall at a height of 60 cm, since bed wall was meant to absorb the solar radiation and transfer it to the air stream. Therefore, the air inside the oven reached a maximum of 47 ℃ and a mean temperature of about 42 ℃. Regarding the air inside the packed bed, the bottom presented lower temperatures than the bed top. This can be explained because the cold air was denser than the hot air, causing a temperature gradient in the air between the glass cover and the fixed bed. As the air velocities were pronounced near the exhaust fan, warm air gets inside, promoting the quick drying of the particles at the top.

According to Silva et al. (20018), in conventional fixed beds there is also a gradient of moisture and temperature through the fixed bed, once the particles near the heated air supply usually dry faster than those farthest away. In this study, the particles near the entrances in the top dried faster than those near the bottom.

Figure 7 – Drying results of SS along the axial positions, after drying in a FO bed configuration: temperatures in the ambient, at the top, bottom and at bed wall for the experiments with (a) 3h of drying; (b) 4 h of drying.
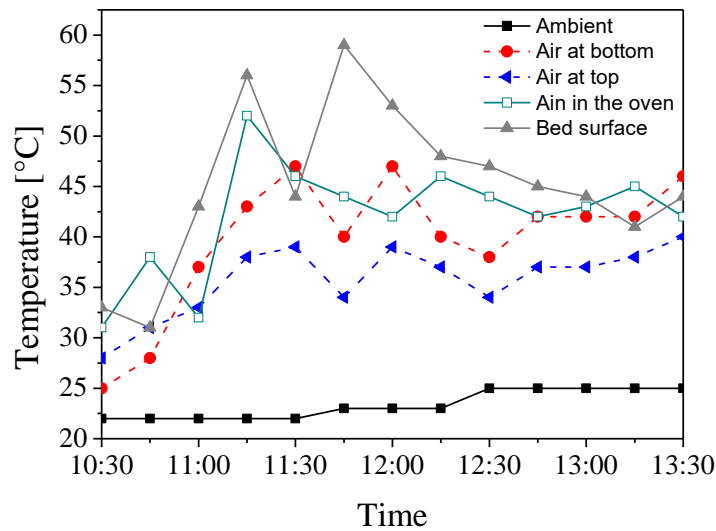
(a) Experiment with 3 h
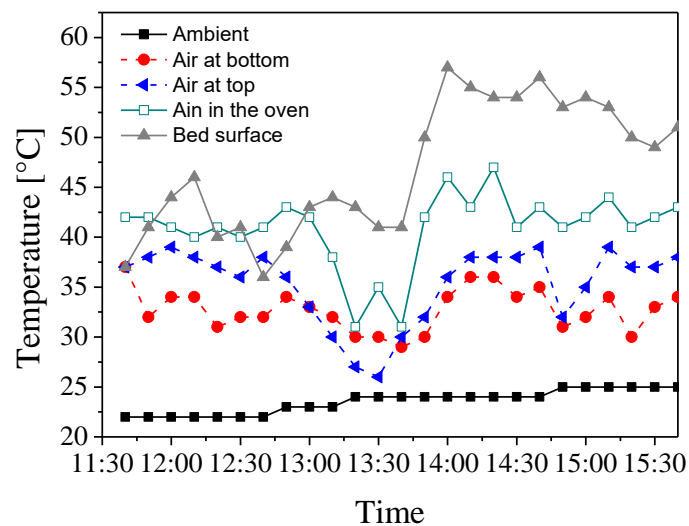
(b) Experiment with 4 h

At the end of drying, the moisture content was evaluated, taking samples near each lateral entrance. Figure 8 compares the axial moisture profile for final drying times of 3 and 4 h. For both experiments, the MR was higher near the exhaust fan, at the bed top, where the material lost about 80% of its initial moisture after 4 h. This occurred due to the elevated air velocity and temperatures observed in this region. In the meantime, at the bottom, the drying was not significant, as the air velocities were not expressive in this region for the FO configuration. Thus, as the simulations indicated, others configurations, such as the AAI and PO configurations, could be more suitable in order to reduce the heterogeneity during the drying.

Figure 8 – Experimental moisture ratio (MR) for the drying of soybean seed for 3h and 4h, at different bed heights.
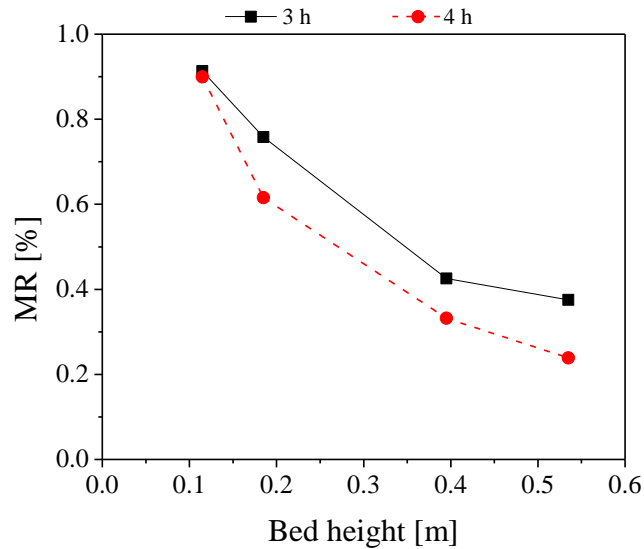
Case 2 – Solar drying of MOL: In this work, MO leaves were dried using the FO and PO fixed-bed configurations. Figure 9 shows the pictures of leaves used in the image analysis before (a) and after (b) the drying process. Although the drying gradient was in the thickness direction, shrinkage of about 20% can be noticed compared with the projected area of the leaves before and after drying.

Figure 9 – The shrinkage effect: comparison between the particles morphology of MOL leaves, before (a) and after (b) drying, using the ImageJ software.
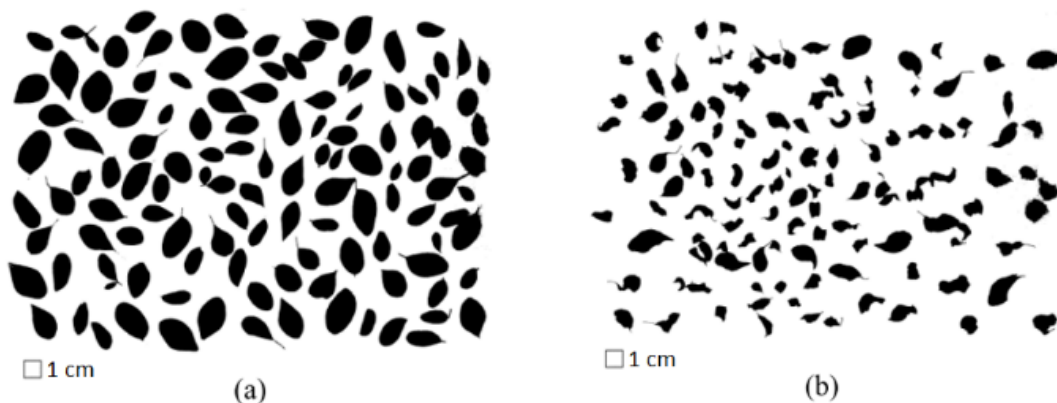
Figure 10a reveals the temperatures measured during the MOL solar drying test for an FO fixed bed. Although the bed temperatures showed a drop at the 3 h and 4 h drying times, the recorded base and top temperatures were the highest among all the tests, which resulted in an excellent reduction of the moisture content. This result agrees with Figure 10b, which

shows the solar radiation changes and the wind velocity during the experiments. Hence, the increases of solar radiation levels coincided with elevations in temperature, especially at the top and bottom; moreover, they were inversely proportional to the increase in wind speed, since the heat losses by convection had decreased the temperature of the solar dryer.

Figure 10c presents the MR as a function of drying time for the FO bed at axial positions of 0.06, 0.13, 0.20, 0.27, and 0.34 m from the bottom. As expected, for all axial positions, a reduction in moisture was observed over the drying time. The upper entrances were also verified to have a more pronounced drying, since they were closer to the outlet. After four hours of drying, shrinkage of the leaves was noticed, about 20%, due to the high temperatures recorded during the day. Thus, the static bed height was reduced, and sampling in the axial positions of 0.27 and 0.34 m was not possible.

To better understand the influence of the air inlets arrangements on the MOL drying, an experiment using PO fixed-bed configuration was also performed. Figures 10d and 10e present the temperatures and the climate conditions against the time, respectively. The solar radiation (632 ± 124 W·m^{-2}) had a greater influence on the bed temperature than the external temperature mainly at the beginning of the drying. The temperature peak (60 °C) occurred at the bed top after 1.5 h of drying in the period of low wind speed (1.5 m·s^{-1}) and high solar radiation (678 W·m^{-2}). The opposite occurred between three and four hours of drying, when an increase of wind speed reduced the bed temperature.

The MR as a function of time can be seen in Figure 10f, for the PO bed. A greater decline in the moisture was noticed for all axial positions, including near the bottom, mainly in the first two hours. The most accentuated drying ($MR = 0.2$) occurred at 0.20 and 0.27 m, near the third airflow inlet, as this entrance had a superior air velocity due to its proximity to the exhaust fan. This agrees with air velocity contours produced by CFD simulations (Figure 6). However, the particles near the bottom still had a smaller drying efficiency, with a final MR of 0.52. Since these particles were behind the first inlet, there was no significant air velocity in this position, as predicted by CFD simulations.

As regards the drying rate (in percentage points per hour, pp·h^{-1}), Figure 11 demonstrates that the PO bed was more efficient than the FO bed configuration, as the PO bed removed about 6 to 9 pp·h^{-1} of moisture, while the FO bed removed less than 2 pp·h^{-1} in axial positions until 0.27 m and a maximum of 5 pp·h^{-1} at the top. This means an increment of about 300% in the drying rate for the PO bed, mainly around the bottom. In addition, the final MR along the bed was similar and almost constant after two hours of drying, showing a sharp decrease in the drying heterogeneity.

Figure 10 – Drying results of MOL leaves with time, at different axial positions: temperatures in the ambient, at the top, bottom and at bed wall for FO bed (a) and (b) PO Bed; solar radiation and wind speed for FO bed (c) and PO bed (d); moisture ratio content for FO bed (e) and PO bed (f).
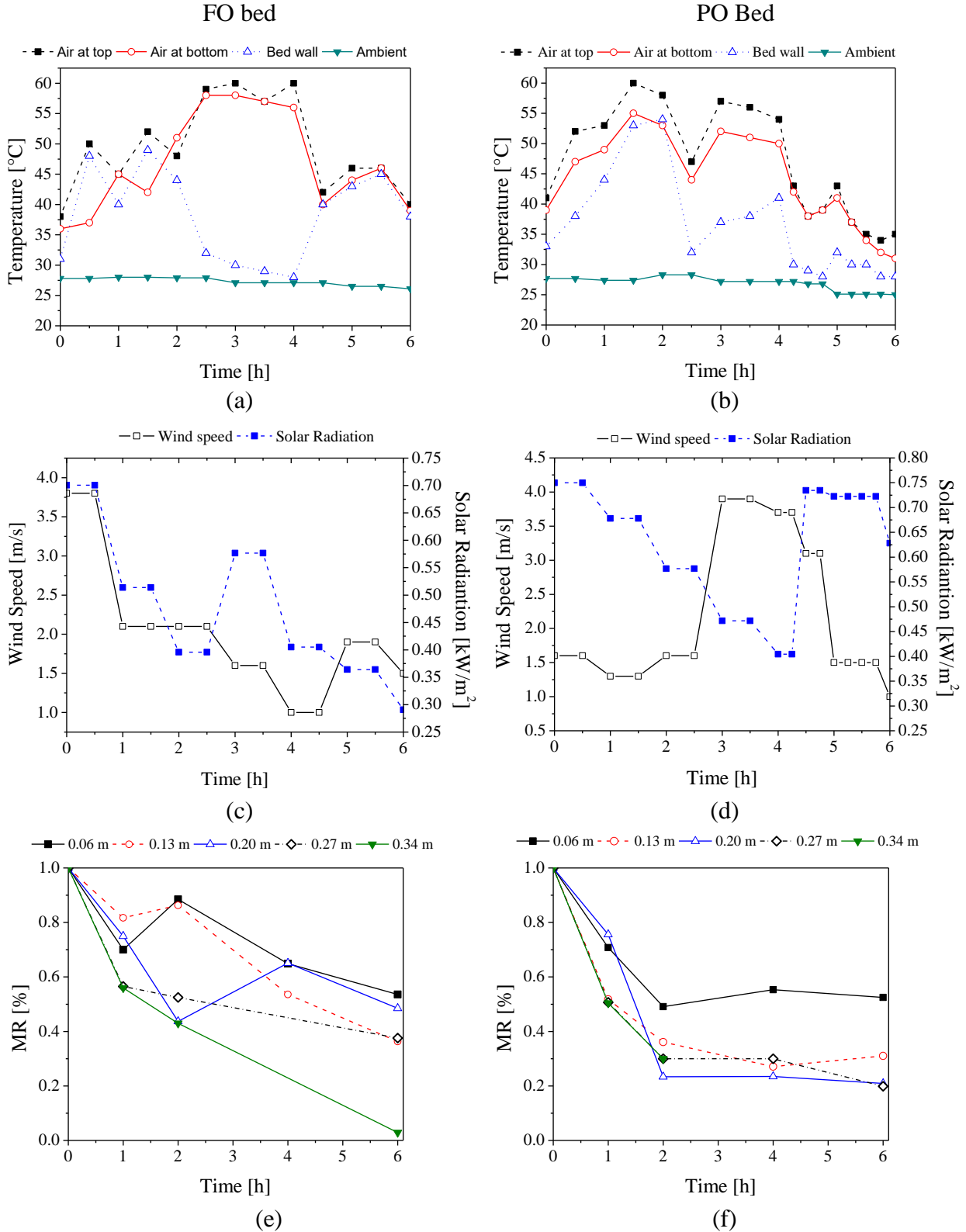
Figure 11 – Comparison between the drying rates of MOL, obtained using the FO bed and PO bed configuration, at different bed heights, in percentage points per hour (pp.h^{-1}).
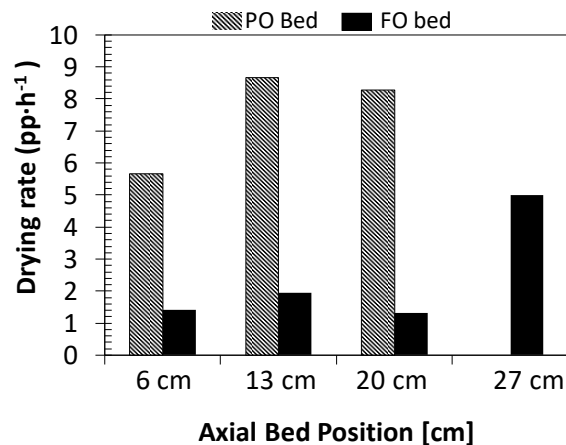
Souza et al. (2015) dried SSs in a conventional fixed bed, heated by electrical resistance, with an air inlet at the bottom and found a maximum drying rate of 2.35 pp·h^{-1}, working with an air velocity of 1 m·s^{-1} and 45 °C. Comparing these results with the present solar dryer, the FO bed configuration achieved similar results of drying rate (2–5 pp·h^{-1}), while the PO bed could remove about 6 to 9 pp·h^{-1} of moisture. Moreover, the conventional fixed bed also showed a strong heterogeneity of the final product, as found in the FO configuration. Therefore, the modifications proposed in this study by CFD simulations could be useful to improve the drying rate by closing the upper entrances, which drastically modified the air fluid dynamics in the porous media and consequently the convective coefficients of heat and mass transfers.

5. Conclusions

In this work, the CFD technique was used to develop new configurations of fixed-bed dryers using solar energy. Regardless of material, the results showed that the fixed bed working with all inlets open (FO bed) achieved similar drying rates compared with conventional fixed-bed dryers (Souza et al., 2015), and a relatively homogeneous dried product was obtained, with the air stream heated by a natural and free energy source.

The CFD simulations also demonstrated some possible changes in the air inlet configurations and showed that closing the upper inlets modified the airflow path through the porous media. Therefore, the PO bed configuration had a more homogeneous air velocity profile in the axial direction, leading to a more homogeneous dry product. Comparing the solar drying experiments of MOL leaves, the PO configuration conducted a more

homogenous solar drying, with a drying rate about 300% higher than the one using the FO configuration, due to the closure of upper inlets. Moreover, temperatures of about 40 and 60°C were achieved, which are appropriate for the drying of temperature-sensitive materials.

The fixed-bed dryers are recommended for agricultural products, which usually present poor flowability due their high angle of repose, low density, and high moisture content. Therefore, this new equipment can be an interesting alternative for drying in small facilities and farms and can be scaled up to increase its capacity.

Acknowledgements

Referências

Agrawal, A. & Sarviya, R.M. (2016). A review of research and development work on solar dryers with heat storage. *Int. J. Sustain. Energy*, 35, 583–605.

Akbulut, A. & Durmuş, A. (2010). Energy and exergy analyses of thin layer drying of mulberry in a forced solar dryer. *Energy*, 35, 1754–1763.

Almeida, R.L.J., Santos, N.C., Pereira, T.S., Queiroga, A.P.R., Silva, V.M.A, Ribeiro, V.H.A., Araújo, R.D.A., Cabral, M.B., Silva, L.R.I. & Borges, E.M.E.S. (2020). Azuki bean drying kinetics: mathematical modeling and thermodynamic properties. *Research, Society and Development*, 9(3), e27932316.

Andrade, W.A., Cruz, G.P., Silva, M.S., Santos, M.F.O., Silva, G.F. & Santos, J.P.L (2020). Synthesis of a tensoative based on oil Moringa Oleífera Lam and formulation of microemulsioned systems for breaking oil water emulsions. *Research, Society and Development*, 9(2), e193922194.

Araújo, B.S.A. & Santos, K.G. (2017). CFD Simulation of Different Flow Regimes of the Spout Fluidized Bed with Draft Plates. *Mater. Sci. Forum*, 899, 89–94.

Atalay, H., Turhan Çoban, M. & Kıncay, O. (2017). Modeling of the drying process of apple slices: Application with a solar dryer and the thermal energy storage system. *Energy*, 134, 382–391.

Barros, S.L., Câmara, G.B., Leite, D.D.F., Santos, N.C., Santos, F.S., Soares, T.C., Lima, A.R.N., Soares, T.C., Oliveira, M.N., Vasconcelos, U.A.A., Albuquerque, A.P. & Queiroz, A.J.M. (2020). Mathematical modeling of drying kinetics of kino bark (Cucumis metuliferus). *Research, Society and Development*, 9(1), e60911608.

Béttega, R., Barrozo, M., Corrêa, R. & Freire, J. (2013). CFD simulation of heat transfer inside packed beds: Evaluation of effective thermal conductivity, *JP Journal of Heat and Mass Transfe*r, 8(2), 137-148 .

Béttega, R., Moreira, M.F.P., Corrêa, R.G. & Freire, J.T. (2011). Mathematical simulation of radial heat transfer in packed beds by pseudohomogeneous modeling. *Particuology*, 9, 107–113.

Bortolotti, C.T., Santos, K.G., Francisquetti, M.C.C., Duarte, C.R. & Barrozo, M.A.S. (2013). Hydrodynamic study of a mixture of west Indian cherry residue and soybean grains in a spouted bed. *Can. J. Chem. Eng.*, 91(11), 1871-1880.

Câmara, G.B., Oliveira, T.K.B., Leite, D.D.F., Soares, T.C., Lima, A.R.N., Vasconcelos, S.H., Barbosa , M.L. & Trigueiro, L.S.L. (2019). Physico-chemical, toxicological and nutritional characterization of dry and in natura Moringa oleifera Lam leaves, *Research, Society and Development*, 8(11), e178111450.

Cunha, F.G., Santos, K.G., Ataíde, C.H., Epstein, N. & Barrozo, M.A.S. (2009). Annatto Powder Production in a Spouted Bed: An Experimental and CFD Study. *Ind. Eng. Chem. Res.*, 48, 976–982.

Cunha, R.N., Santos, K.G., Lima, R.N., Duarte, C.R. & Barrozo, M.A.S. (2016). Repose angle of monoparticles and binary mixture: An experimental and simulation study. *Powder Technol.*, 303, 203–211.

Ergun, S. (1952). Fluid Flow Through Packed Column, *Chem. Eng. Prog.*, 48(2), 89-95.

Gomes, M.E.M., Albuquerque, A.P., Rodrigues, T.J.A., Wanderley, D.M.A., Rocha, A.P.T. & Silva, O.S. (2020). Prediction of kinetic models for drying lemon balm leaves in a convective dryer. *Research, Society and Development*, 9(2), e86922052.

INPE (2017). Brazilian Atlas of Solar Energy. http://labren.ccst.inpe.br/atlas_2017-en.html.
Krawczyk, P. & Badyda, K. (2011). Two-dimensional CFD modeling of the heat and mass transfer process during sewage sludge drying in a solar dryer, *Archives of Thermodynamics*, 32, 3–16.

Leon, M.A. & Kumar, S. (2008). Design and Performance Evaluation of a Solar-Assisted Biomass Drying System with Thermal Storage. *Dry. Technol.*, 26, 936–947.

Mardiyani, S.A., Hadi Sumarlan, S., Dwi Argo, B. & Setyo Leksono, A. (2019). Design of Eco-friendly Fixed Bed Dryer Based on A Combination of Solar Collector and Photovoltaic Module, *Nature Environment and Pollution Technology*, 18(1), 21-30.

Müller, C.R., Scott, S.A., Holland, D.J., Clarke, B.C., Sederman, A.J., Dennis, J.S. & Gladden, L.F. (2009). Validation of a discrete element model using magnetic resonance measurements. *Particuology*, 7(4), 297–306.

Vieira Neto, J.L., Duarte, C.R., Murata, V. V. & Barrozo, M.A.S. (2008). Effect of a Draft Tube on the Fluid Dynamics of a Spouted Bed: Experimental and CFD Studies. Drying Technol., 26(3), 299–307.

Olabode; Z., Olunlade, B., Akanbi, C. & Adeola, A. (2015). Effects of Drying Temperature on the Nutrients of Moringa (Moringa oleifera) Leaves and Sensory Attributes of Dried Leaves Infusion. *Direct research journal of agriculture and food science*, 3(5), 117–122.

Perumal, S., Klaus, B., 2003. Antioxidant Properties of Various Solvent Extracts of Total Phenolic Constituents from Three Different Agroclimatic Origins of Drumstick Tree (Moringa oleifera Lam.) *Leaves. J. Agric. Food Chem.*, 51(8), 2144–2155.

Ratti, C. & Mujumdar, A.S. (1997). Solar drying of foods: Modeling and numerical simulation. *Solar Energ*y, 60, 151–157.

Rigueto, C.V.T., Nazari, M.T., Evaristo, L.M., Rossetto, M., Dettmer, A., Geraldi, C.A.Q. & Piccin, J.S. (2020). Influence of foam-mat drying temperature of red jambo (Syzygium malaccense). *Research, Society and Development*, 9(3), e40932382.

Santos, A.R.A., Cruz, L.A. & Gontijo, H.M. (2019). Study of water and sewage systems in the rural community of Capela Branca in Bela Vista de Minas/MG. *Research, Society and Development*; 8(2), e4782740.

Santos, K.G., Francisquetti, M.C.C., Malagoni, R.A. & Barrozo, M.A.S. (2015). Fluid Dynamic Behavior in a Spouted Bed with Binary Mixtures Differing in Size. *Drying Technology*, 33(14), 1746–1757.

Santos, K.G., Santos, D.A., Duarte, C.R., Murata, V.V., Barrozo, M.A.S. (2012). Spouting of Bidisperse Mixture of Particles: A CFD and Experimental Study, *Drying Technology*, 30, 1354–1367.

Santos, N.C., Leite, D.D.F., Câmara, G.B., Barros, S.L. & Santos, F.S. (2020a). Mathematical modeling of drying kinetics of grapefruit peels (*Citrus paradisi Macf.*).*Research, Society and Development*, 9(1), e61911609.

Santos, N.C., Almeida, R.L.J., Pereira, T.S., Queiroga, A.P.R., Silva, V.M.A., Amaral, D.S., Almeida, R.D., Ribeiro, V.H.A., Barros, E.R. & Silva, L.R.I. (2020b) Mathematical modeling applied to the drying kinetics of pitomba bark (Talisia esculenta). *Research, Society and Development*, 9(2), e46921986.

Silva, D.I.S., Nogueira, G.D.R., Duzzioni, A.G. & Barrozo, M.A.S. (2013). Changes of antioxidant constituents in pineapple (Ananas comosus) residue during drying process. *Ind. Crops Prod.*, 50, 557–562.

Silva, D.I.S., Souza, G.F.M.V. & Barrozo, M.A.S. (2019). Heat and mass transfer of fruit

residues in a fixed bed dryer: Modeling and product quality. *Drying Technology*, 37(10), 1321–1327.

Silvério, B.C., Santos, K.G., Duarte, C.R. & Barrozo, M.A.S. (2014). Effect of the Friction, Elastic, and Restitution Coefficients on the Fluid Dynamics Behavior of a Rotary Dryer Operating with Fertilizer. *Ind. Eng. Chem. Res.,* 53(21), 8920–8926.

Souza, G.F.M.V., Miranda, R.F., Lobato, F.S. & Barrozo, M.A.S. (2015). Simultaneous heat and mass transfer in a fixed bed dryer. *Appl. Therm. Eng.*, 90, 38–44.

Souza, G. F. M. V., Miranda, R.F., Barrozo, M.A.S. (2015). Soybean (*Glycine max* L. *Merrill*) Seed Drying in Fixed Bed: Process Heterogeneity and Seed Quality. *Drying Technolog*y, 33(14), 1779–1787.

Tegenaw, P. D., Gebrehiwot, M. G. &Vanierschot, M. (2019). On the comparison between computational fluid dynamics (CFD) and lumped capacitance modeling for the simulation of transient heat transfer in solar dryers. *Solar Energy*, 184, 417–425.

Vieira, L.G.M., Silva, D.O. & Barrozo, M.A.S. (2016). Effect of Inlet Diameter on the Performance of a Filtering Hydrocyclone Separator. *Chem. Eng. Technol.*, 39(8), 1406–1412.

Vieira Neto, J.L., Costa, D.D.L., Souza, L.V., Pires, R.F., Souza, D.L., Silvério, B.C. & Santos, K.G. (2017). A Fluid Dynamic Study in a Rotating Disk Applied in Granulation of Fertilizers. *Mater. Sci. Forum*, 899, 142–147.

Porcentagem de contribuição de cada autor no manuscrito

Ana Carolina Ribeiro Stoppe – 34%

José Luiz Vieira Neto – 33%

Kássia Graciele dos Santos – 33%